EUROfusion

EUROFUSION WPMAT–PR(15)19

F. Jiménez et al.

A GPU-Based Parallel Object Kinetic Monte Carlo Algorithm for the Evolution of Defects in Irradiated Materials

Preprint of Paper to be submitted for publication in
Computational Materials Science

This work has been carried out within the framework of the EUROfusion Consortium and has received funding from the Euratom research and training programme 2014-2018 under grant agreement No 633053. The views and opinions expressed herein do not necessarily reflect those of the European Commission.

A GPU-based parallel Object kinetic Monte Carlo algorithm for the evolution of defects in irradiated materials

F. Jiménez[a], C.J. Ortiz[a]

[a]*Laboratorio Nacional de Fusión por Confinamiento Magnético - CIEMAT. Avenida Complutense 40, E-28040 Madrid, Spain*

Abstract

In this work we present a parallel Object kinetic Monte Carlo (OkMC) computational model implemented using GPUs (graphics processing units) computing to simulate the evolution of interacting random walkers in materials. Different test simulations were performed under different conditions and compared to analytical solutions and sequential OkMC codes. The simulation results obtained with our algorithm show to be in excellent agreement with sequential OkMC codes and analytical solutions. The speedups reached with the GPU programming with respect to sequential OkMC codes in the test cases used here were in the range [30-40]. This increased efficiency allows to follow the evolution of millions of interacting particles in a relatively short computational time in contrast to classical OkMC codes. We expect this parallel kMC algorithm based on GPU programming to allow for investigations on defect evolution in materials using simulation boxes of realistic dimentions and physical times close to those achieved experimentally.

Keywords: Kinetic Monte Carlo, GPU, defect evolution, Parallel computing

1. Introduction

Many properties of solids, such as hardness [1], ductile-to-brittle transition temperature [2], conductivity [3, 4] or tensile strength [5] are related to the presence of defects or impurities, in particular when they are out-of-equilibrium conditions. This occurs for instance when impurities are directly implanted such as in the semiconductor industry for the fabrication of transistors, or when the material is subject to neutron irradiation such as in fission reactors or in the future fusion reactors.

Therefore, simulating the spatial and temporal evolution of defects and impurities in materials irradiated or under irradiation conditions is essential to

Email address: christophe.ortiz@ciemat.es (C.J. Ortiz)

understand and predict their macroscopic properties and behaviour in non-equilibrium conditions. To do so, different models or numerical approaches can be used like Molecular Dynamics (MD) [6, 7, 8, 9, 10, 11], kinetic Monte Carlo (kMC) [12, 13, 14, 15, 16, 17, 18, 19] or mean field rate theory [15, 20, 21, 22, 23, 24] (also sometimes called Cluster Dynamics). Each of these methods has advantages and drawbacks and allows to address different scales of time and space. In this paper we focus on kMC models.

In particular, in this work we shall focus on a subset of kMC denominated Object kMC (OkMC), which only follows the evolution of off-lattice defects, such as impurities, interstitials or vacancies or their clusters thereoff. This method has been widely used to simulate the evolution of defects or impurities in different materials and fields of research [25, 15, 26, 27, 28, 29, 30]. In this simulation framework, each object (defect or impurity) possesses a set of characteristics such as type, shape, migration energy or binding energy to other defects, which determine the rate of the events it can undergo [31, 12, 13, 15, 27]. It must be noted that the OkMC cannot predict the rate of events, they must be given a priori [25]. In this respect, the rate of events is mainly determined by the migration and binding energies of defects and can usually be accurately calculated using First-Principle calculations [32, 33, 34, 35] and/or MD [36, 37, 38, 39]. Since OkMC keeps the coordinates of each defect, it allows to account for spatial correlations between individual defects in the system [27], which is an advantage over other models such as the Rate Theory [15, 40], which are based on a mean-field approximation. Moreover, since only off-lattice defects are followed, in contrast to MD that simulates the motion of every atom in the simulation box, OkMC models are not limited to short times [41] like MD but can reach physical times closer to those achieved experimentally. This makes OkMC a valuable tool for the investigation of defect kinetics in irradiated materials in quasi-realistic conditions.

OkMC models are based on the Bortz-Kalos-Leibowitz (BKL) algorithm [42] also known as *residence-time* algorithm. This algorithm is equivalent to the stochastic simulation algorithm (SSA) developed by Gillespie [43]. According to this algorithm, a list of all possible event rates (the frequency line) is first formed. An event to carry out is selected randomly from the frequency line. Then, one of the particles that can undergo the selected event is chosen randomly and the event is carried out. Physical time is then advanced using a Poisson law to calculate the probable time interval that might have passed between two events. The procedure is then repeated until a specified physical time has been reached. Since only one event is carried out at each time step, OkMC models become computationally intensive [44] when the evolution of a large amount of defects must be simulated. For this reason, most OkMC codes using the standard BKL algorithm are usually limited to relatively small simulation boxes [45], in the order of $(200a_0)^3$, where a_0 is the lattice constant, in order to restrict the amount of particles to follow. Clearly, this strong restriction seriously hinders the study of defect evolution in realistic pieces of materials that can contain polycrystals and grain boundaries, which play an important role in the evolution of defects and/or impurities and thus, cannot be neglected [46, 47, 48, 49, 50, 51].

Furthermore, small simulation boxes are inadequate to investigate the evolution of defects that form at low densities. This is the case for instance of dislocation loops (DLs) that form in irradiated Fe. For example, Arakawa et al [52] observed that DLs form in Fe under electron irradiation at densities of about $10^{22} - 10^{23}\ m^{-3}$. This means that with a typical OkMC simulation box with a volume of $(200a_0)^3$, it is only possible to follow the evolution of 1 to 20 DLs, which is clearly not enough statistical information for the prediction of defect evolution and their influence on a macroscopic level.

In order to address the evolution of defects in realistic conditions using the BKL algorithm, it seems thus unavoidable to increase the simulation box volume. This implies a significant increase of the number of particles to follow (at constant density), and, as a consequence, of the computational effort. Therefore, it is desirable to find some way to accelerate the BKL algorithm. For example, Martínez et al [53] recently proposed a parallel version of the BKL algorithm using a multi-processors approach and the Message Passing Interface (MPI) paradigm. Though the authors observed a speedup of the algorithm, they observed that the achieved speedup tends to saturate as the number of processors increases, due to the increase of communication between processors.

In this work we present an alternative parallel BKL algorithm that we implemented using GPU (graphics processing unit) programming. Owning to their architecture, GPUs are capable of processing many data at the same time, so they are ideal for solving parallelisable problems [54]. For example, the NVIDIA® GeForce® GTX TITAN Black that we used in this work features 15 multiprocessors with 192 cores per multiprocessor, which yields a potential maximum of 240 concurrent blocks of 128 threads per block, i.e. 30720 concurrent threads. As one can see, the parallelism that can be reached with a single graphics card is important, which explains why general-purpose programming on graphics processing units (GPGPU) has risen in recent years [55] as a reliable and interesting alternative to inherently sequential CPU coding, especially in scientific computation. In addition, GPUs are known as energetically efficient devices as fewer watts per byte are needed than for CPUs.

The present article is organised as follows. In section 2 we describe our parallel version of the BKL algorithm and highlight its advantages. In section 3 different numerical tests are performed to validate our GPU-OkMC model. In particular, results are compared to those obtained with a CPU-based OkMC, as far as accuracy and performance are concerned. Finally, in order to demonstrate the efficiency of our GPU-OkMC, we reproduce a typical resistivity recovery experiment in Fe, which is a relevant problem in materials science [15, 38, 56, 57, 58, 59].

2. parallel OkMC algorithm

In this section we describe our parallel version of the BKL algorithm, which was implemented using the high parallelism offered by GPUs.

First, a particle array that resides in the global memory of the GPU is built and distributed in the simulation box. Then, the following operations are

performed in parallel.

1. For each particle p_i able to undergo different events E_k with rate r_k, the sum of event rates is computed in parallel, as described by:

$$R_i = \sum_{k=1}^{q_i} r_k \tag{1}$$

   with q_i being the total number of events that particle p_i can undergo.
2. The maximum sum of event rates R_{max} of all particles is determined in a parallel manner:

$$R_{max} = max\{R_i\} \tag{2}$$

3. Global time is advanced by the time step:

$$\delta t = \frac{\omega}{R_{max}} \tag{3}$$

   where $\omega > 0$ is a real number.
4. For each particle p_i, the number of times N_k that each event E_k with rate r_k will occur during the time step δt is determined using the Poisson distribution:

$$P(r_k, N_k; \delta t) = \frac{1}{N_k!} \left(r_k \delta t\right)^{N_k} \exp(-r_k \delta t) \tag{4}$$

5. Particles undergo the selected events in parallel, provided $N_k > 0$.
6. The surrounding of particles that have moved is analysed.
7. Particles that lie within a specified distance interact, provided interaction is allowed.

Here, we would like to emphasise the main differences between our parallel kMC algorithm and the original BKL [42] and the parallel algorithm proposed by E. Martínez [53]. On one hand, in the standard BKL algorithm, only one event is performed during each time step. In the case of the parallel algorithm from Martínez et al developed using MPI, at most N_{proc} (number of processors used) events can occur during the same time step due to the subdivision of space into N_{proc} subdomains. In our algorithm, space is not divided into subdomains. Instead, we consider that all particles are potentially able to undergo events during each time step, the probility of which being determined by the Poisson distribution (see Eq. 4). In practice, this significantly increases the number of events that can occur in parallel during each time step. Therefore, the use of a GPU and the high parallelism it offers is necessary. Since the probability of each event (for each particle) explicitely depends on the time step (see Eq. 4), it is first necessary to fix a value for the time step before events are carried out. In contrast, in the standard BKL or in the algorithm developed by Martínez et al, events are first carried out and then the probable time interval that might have passed between two events is calculated according to a Poisson law. Since each particle in our algorithm is considered, the time step that is selected must

be independent of the total number of particles in the system. Furthermore, the time step cannot be arbitrary but must limited by the highest event rate (step 2) in the system in order to preserve accuracy. Therefore, a natural choice is a time step that is inversely proportional to the highest sum of event rates in the system (Eq. 2). On one hand, the ω value must be large enough so that a significant number of events can occur during each time step. On the other hand, the selection of the ω value must be small enough so that the system as a whole does not change significantly and so that physical accuracy is preserved. This issue is similar to that encountered in the tau-leaping method that was proposed by Gillespie[60] and will be addressed in subsection 2.1.

Once the events selected have been realised in parallel, the surrounding of each particle that has moved must be analysed in order to determine the possible interaction partners. This corresponds to steps 6-7. As it is usually done in other OkMC models [31, 12, 27, 15], in our model we assume that a reaction between two particles instantaneously takes place whenever two particles lie within a distance r_c, called the capture radius. This reflects the fact that the interaction range is limited and that the necessary time for a reaction to occur when species are close is much shorter than any diffusion process and can thus be seen as instantaneous. Following this assumption, only the close surrounding of those particles that have undergone an event is physically interesting and must be analysed. In practice, the distance between the particles that have moved and the other particles must be calculated to check whether they lie within the capture radius and could thus undergo a reaction. This step could be computationaly costly if all the distances between neighbours had to be calculated at each time step. To avoid this, we used the collision detection algorithm that is described in chapter 32 of the book GPU Gems 3 [61]. According to this algorithm, protective spheres are drawn around each particle with radii equal to the largest capture radius of their defined interactions where they may be respectively involved. The cell where the particle centre is located is labelled 'home cell' while cells intersecting its protective sphere are called 'phantom cells'. In order to avoid unnecessary searches for interaction partners through the whole system, space is divided into subdomains with a size that is at least larger than twice the largest capture radius r_c. This way, distances between particles are only calculated for particles belonging to the same subdomain (be it as 'home' or 'phantom' cells, for further reference see [61]), significantly reducing the computational effort. Owing to the division of space into subdomains, the inspection of the surrounding of each particle that has moved can clearly be achieved in parallel and independently in the GPU. In order to perform the calculation of distance between pairs of particles within a given subdomain and determine the possible interactions between particles, we used the GPU concept of thread blocks. The advantage of thread blocks is that the different threads they are composed of share the same block of shared memory, whose access is significantly faster than the one to the global memory. In our implementation, each thread block is assigned a subdomain and each thread of the block is in charge of the calculation of the distance between the particle that has moved and another particle within that subdomain. This way, the calculation of distances between

possible interacting pairs is achieved in parallel, which significantly accelerates calculations. After the calculation of distances between potential interacting pairs have been achieved, it could happen that various particles lie within a distance lower than the capture radius. Thus, a criterion is necessary to decide which pairs should interact. At this point, several criteria can be considered. The most intuitive one is that the closest pair is preferential over the others and should be the one to indeed react. Although this criterion seems logical, from the physical point of view, there is no evidence that reactions really take place this way and there are probably other factors to take into account, such as the energy landscape (shape of the interaction potential) between the different particles in presence. Another criterion is simply to consider, among all the particles within the capture radius, the first pair that appears in the list. This somehow takes into account the stochasticity of reactions and the fact that the energy landscape between particles cannot be known a priori. In this work, we chose to use a combination of both criteria. Particles in the same thread block are iterated through and allowed to react with the closest neighbour within the capture radius. The reaction thus takes place for this pair of particles, should they reside within the capture radius. This step is iteratively applied to the rest of particles in the thread block until all potential interacting pairs have reacted.

2.1. Selection of the time step

As we mentioned previously, in our algorithm the time step must be first fixed in order to calculate the probability that each particle has to undergo an event. Since each particle is considered separately from the others and at the same time, the time step must not depend on the number of particles in the system, in contrast to what is done in the standard BKL or in the Martínez algorithms. Indeed, in the original BKL algorithm, the probable time interval that might have passed between two events is inversely proportional to the sum of the event rates in the system. It thus somehow depends on the total number of particles in the system. If, for instance, we consider a simple system composed of N_{part} identical particles that can only perform one type of transition with event rate r, then the time step achieved in the standard BKL algorithm is simply given by:

$$\delta t_{BKL} = \frac{-\log(\zeta)}{N_{part} \cdot r} \tag{5}$$

where $\zeta \in (0, 1]$ is a uniform random variable. According to Eq. 5 we can see that the time step in the BKL algorithm gets smaller as the number of particles in the system increases. Furthermore, it can be proven that, if $X := -\log(\zeta)$, then X is distributed as an exponential distribution with mean value $\lambda = 1$. Provided the number of time steps is large enough in the simulation, the average time step in the BKL algorithm is thus:

$$\delta t_{BKL} \approx \frac{1}{N_{part} \cdot r} \tag{6}$$

In our algorithm, the time step value is related to the particle that displays the largest sum of event rates, according to Eqs. 2 and 3, and is thus independent of the number of particles in the system. Thus, if we consider the previous system of N_{part} identical particles, the time step achieved with our algorithm is simply $\delta t = 1/r$ and is in average N_{part} times larger than the one achieved with the standard BKL algorithm. In practice, this means that for typical systems containing several hundred thousands or millions of particles, with our algorithm the time step value is several orders of magnitude larger than that achieved with the standard BKL algorithm. This strongly reduces the number of computational steps that are necessary to reach a specified physical time. However, due to the large values that the time step can take in our algorithm, there exists a significant probability that a particle undergoes several times the same event during the same time step. This can be clearly seen in Fig. 1 where we plotted the probability (Eq. 4) that an event E with rate r occurs N times during the same time step. Here we have assumed a time step $\delta t = 1/r$, i.e. $\omega = 1$ in Eq. 3.

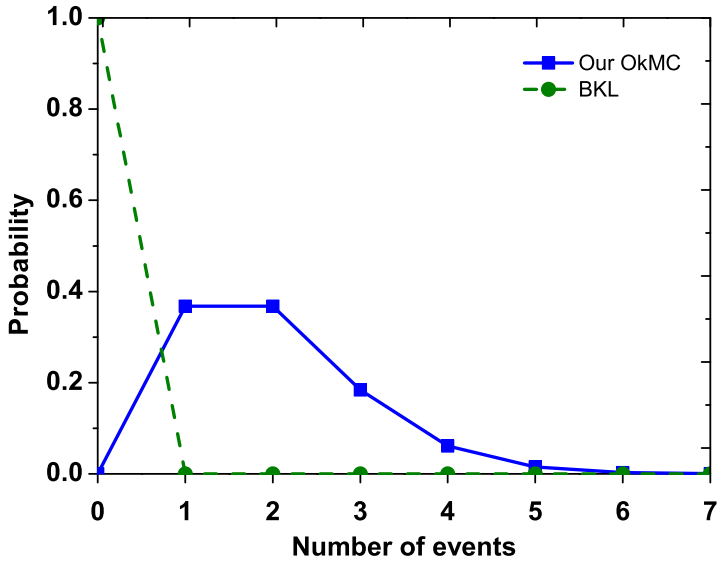

Figure 1: Probability that a particle performs a given number of events during a time step in our algorithm (closed squares) and in the BKL algorithm (open triangles).

For comparison, we also reported the probability of events for the standard BKL algorithm, assuming a typical system containing $N_{part} = 200000$ identical particles and the average time step given by Eq. 6. As one can see, in the standard BKL algorithm, the probability that a particle undergoes no event

at all during a time step is close to 1 whereas the probability that a particle undergoes one event is N_{part} times smaller, i.e. orders of magnitude smaller. Furthermore, the probability that a particle undergoes K times the same event during the same time step becomes negligible as it varies with $1/N_{part}^K$. This explains why in the BKL algorithm only one particle in the system experiences one event during a time step. In contrast, in our algorithm, the time step is such that the probability that an event occurs during a time step $\delta t = 1/r$ is relatively high (~ 0.37), as can be seen in Fig. 1. This implies that a large fraction of particles in the system can undergo an event during the same time step. The probability that the event occurs two and three times is also non-negligible as we can see in Fig. 1. However, since the surrounding of particles is only examined after the time step has passed, this might affect the accuracy of the solution. For instance, a large time step may allow a particle to undergo N migrations during the time step and to ignore its surroundings, and thus possible interactions, on $N_m - 1$ occasions. This might affect accuracy at large concentrations for which the distance between particles can be relatively small. In order to achieve a physically realistic approximation, this occurrence ought to be minimised. As mentionned previously, this problem is also encountered in the tau-leaping method [60] developed by Gillespie. By simply choosing small values of ω (Eq. 3), i.e. small values of the time step, it is in principle possible to minimise the effects of this approximation, as can be seen in Fig. 2. In this figure we plotted the probability (Eq. 4) that an event occurs several times during the same time step for different values of ω. As it is evidenced, this probability significantly decreases as the ω value does. For instance, for $\omega = 0.1$, the probability that an event occurs twice during the time step is already negligible. On the other hand, it is desirable to find a compromise and select a time step that is sufficiently large in order to keep a substantial simulation performance. However, it must be noted that in the different cases that we studied here, we did not observe a significant influence of ω on the result accuracy. Therefore, in the rest of the document, all simulations were performed taking $\omega = 1$, i.e $\delta t = 1/R_{max}$. Furthermore, it seems natural to choose this value for ω since, according to the Poisson distribution properties, it corresponds to one event on average per time step for the particles that exhibit the highest sum of event rates.

3. Test cases

In this section, we show some test results simulated using our parallel OkMC algorithm. The OkMC model that we described in previous section was implemented using the programming framework CUDA 6.5 (Compute Unified Device Architecture). CUDA is an extension of C/C++ that was introduced by NVIDIA® in 2007 for graphics cards. The simulations shown here were performed on a NVIDIA® GeForce® GTX TITAN Black card with 6 GB of global memory and 2880 CUDA cores. As practical cases, tests were performed considering the evolution of self-interstitial atoms (SIA) and vacancies (V) in Fe.

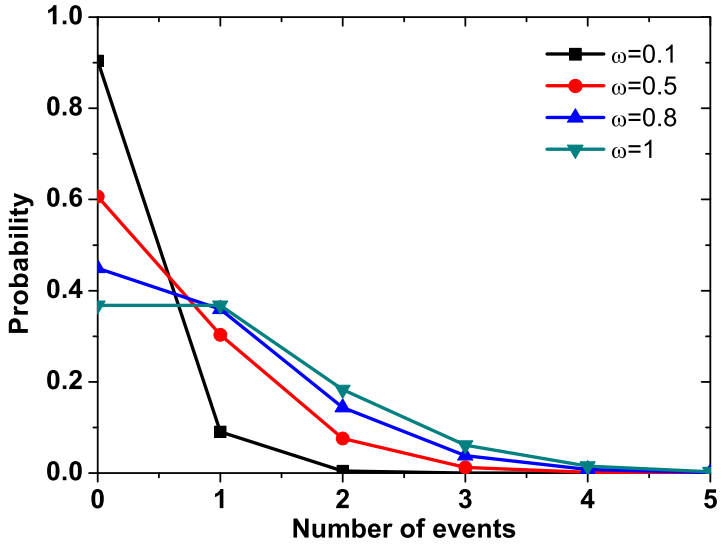

Figure 2: Probability that a particle performs a given number of events during the time step δt for different values of ω.

3.1. Random walks of non-interacting particles

Since the evolution of defects in materials often occurs by means of random walks, here we simulated the diffusion of a large amount of non-interacting particles. In this simple case, results can be compared with analytical solutions. We simulated the random walk of five million SIAs in a $(36a_0)^2 \times 216a_0$ ($a_0 = 2.86\mathring{A}$) box and initially located in a plane at $z = \frac{z_{max}}{2}$, with their x, y positions $0 \leq x \leq x_{max}$ and $0 \leq y \leq y_{max}$ being initially random. By letting these particles perform a one-dimensional random walk in the z direction, after a time t we expect their profile in said direction to describe a Gaussian function in accordance to Fick's laws of diffusion, provided the number of jumps is sufficiently high. This test was carried out assuming an attempt frequency $\nu_0 = 10^{13}\ s^{-1}$ and a migration energy $E_m = 0.34\ eV$, which corresponds to the parameters of the SIA in Fe[32]. According to these parameters, the rate of the unique event (jump) that can occur in the system is:

$$r = \nu_0 \cdot exp\left(-\frac{E_m}{k_B T}\right) \tag{7}$$

where k_B is the Boltzmann constant and T the temperature in K.

Simulations were performed for temperatures of $T = 130$, 135 and 140 K and a time $t_{max} = 30\ s$. Our results are reported in Fig. 3 and compared to a

Gaussian function that represents the probability to find a particle between z and $z + \delta z$ after a time t [62]:

$$Prob(z,t) \cdot \delta z = \frac{1}{2(\pi D t)^{\frac{1}{2}}} \cdot \exp\left(-\frac{z^2}{4Dt}\right) \cdot \delta z \tag{8}$$

where D is the macroscopic diffusion coefficient of SIAs that is defined using the attempt frequency ν_0 and the migration energy E_m as follows:

$$D = \frac{\nu_0 \lambda^2}{2} \exp\left(-\frac{E_m}{k_B T}\right) \tag{9}$$

where λ is the jump length. The factor 1/2-instead of the typical 1/6-corresponds to random walks in one dimension, as it is assumed here. As one can see in Fig. 3, results obtained with our GPU-OkMC are in very good agreement with the analytical solution.

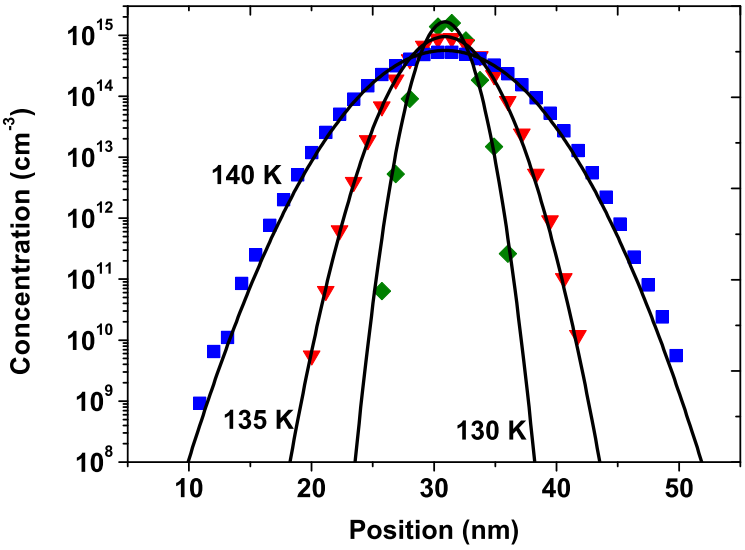

Figure 3: Comparison between the 1D profiles resulting from the diffusion of five million particles during 30 s for three different temperatures as simulated by our GPU-based OKMC code (symbols) and the analytical solution (lines).

3.2. Diffusion of non-interacting particles in the presence of absorbing surfaces

Next test case involves the random walk of non-interacting particles in the presence of absorbing surfaces. This case if of high relevance in irradiated materials as point defects that are created by displacement cascades, such as interstitials and vacancies, tend to recombine when they reach the surface.

In this case, we simulated the evolution of five million SIAs initially distributed randomly in the simulation box and allowed to perform random walks in the three dimensions during 200 s for different temperatures. The volume of the simulation box was $(400a_0)^3$. Periodic boundary conditions were assumed in x and y directions whereas absorbing boundary conditions were assumed at $z = 0$ and $z = 400a_0$. The same jump frequency and the migration energy were used to calculate the event rate (jump) as in previous subsection. In order to validate our GPU-OkMC model, simulations with classical diffusion equations and Dirichlet boundary conditions were also performed. Fig. 4 shows the evolution of the total number of particles with respect to time for the different temperatures. For comparison, we also reported the results obtained with the classical diffusion equations. As we can see, the results obtained with our GPU-OkMC model are in excellent agreement with those obtained with diffusion equations. In the same way, Fig. 5 shows the depth profiles of particles for the different temperatures considered here. The very good agreement obtained with the diffusion equations clearly evidences that our GPU-OkMC accurately accounts for the recombination of particles on absorbing surfaces.

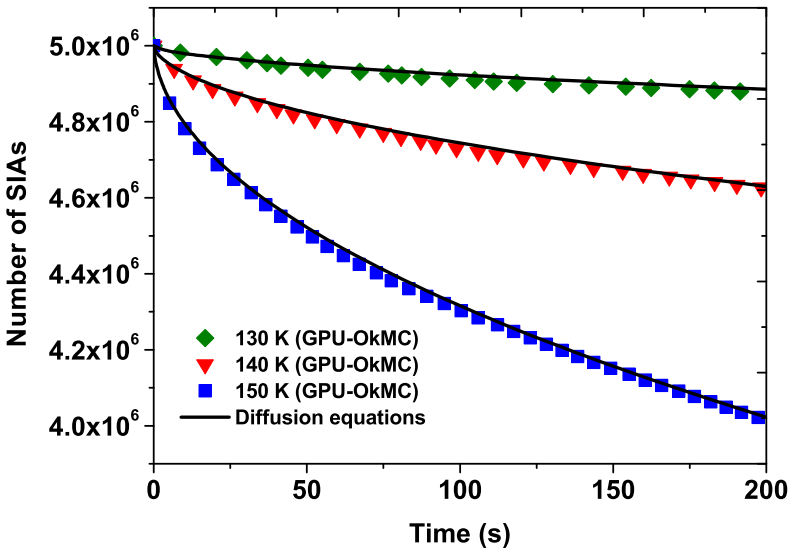

Figure 4: Evolution of the total number of random walkers as a function of time in the presence of two absorbing surfaces. GPU-OkMC results (symbols) are compared to those obtained with diffusion equations (lines).

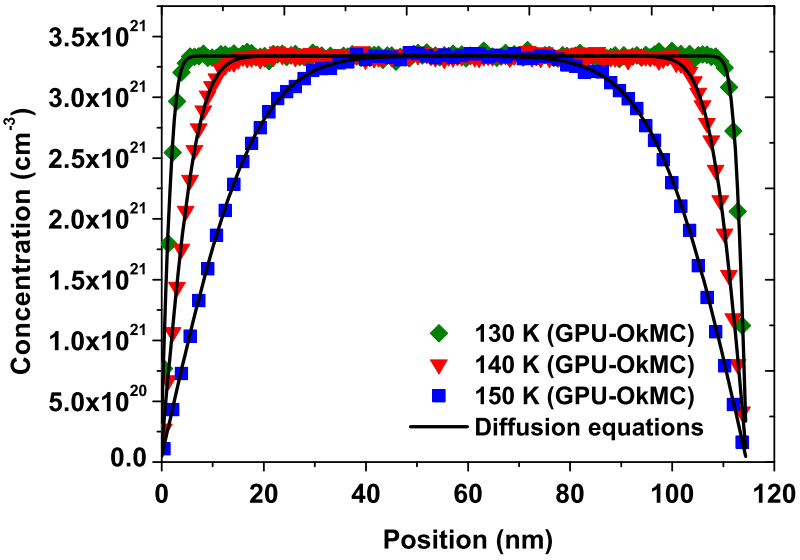

Figure 5: Depth profiles of particles in z direction for three different temperatures. GPU-OkMC results are represented by symbols while those predicted by diffusion equations are represented by lines.

3.3. Recombination of interacting particles

In this subsection we address the case of interacting random walkers, which is of high interest in many fields of research. Indeed, the evolution of many systems observed in biology, chemistry or in irradiated materials is often determined by the kinetics of diffusion-limited reactions $A + B \rightarrow AB$. As explained in section 2, it is assumed that particles A and B instantaneously react if the distance between both is smaller than r_c. As a practical case of interest, here we shall consider the case of the annihilation of SIAs and vacancies that form by collision cascades in irradiated Fe. This can be represented by the reaction $I + V \rightarrow 0$. The same physical parameters (attempt frequency and migration energy) as in previous subsections were used for SIAs to calculate the event rate corresponding to the jump frequency. To calculate the jump frequency of vacancies in Fe, we used a migration energy of 0.67 eV [32, 15] and the same attempt jump frequency as for SIAs. Regarding the capture radius for the annihilation reaction, a value of $3.3a_0$ was used to describe the range of interaction between interstitials and vacancies, as it is commonly accepted in the community [32, 15].

We considered the diffusion and recombination of 4 million SIAs and 4 million vacancies initially randomly distributed in a hypothetic Fe material with volume size of $(200a_0 \times 200a_0 \times 70000a_0)$. This corresponds to a material with a thickness of about 20 μm, i.e. of realistic dimensions. The evolution of the

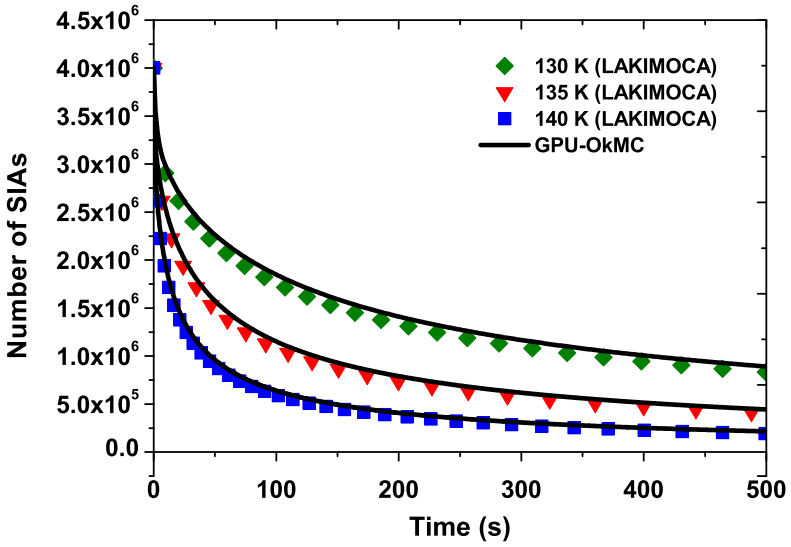

Figure 6: Evolution of the number of SIAs as a function of time for different temperatures. Results are compared to those obtained by the sequential OkMC LAKIMOCA (courtesy of C. Domain).

system was simulated for temperatures of 130, 135 and 140 K for 500 s. Periodic boundary conditions in all directions were assumed. Thus, in the present case, particles can only disappear by recombination. For comparison of accuracy and performances, simulations were also performed using a sequential (CPU) OkMC code, i.e. based on the standard BKL algorithm. For this, LAKIMOCA[31] code version o128p was used. LAKIMOCA simulations were performed on a CPU AMD Opteron 6174@2.2Ghz. In Fig. 6 is shown the evolution of the number of SIAs as a function of time for the different temperatures considered here. The results obtained with the sequential OkMC LAKIMOCA are also reported for comparison. Clearly, the agreement between both models is excellent, which again validates our parallel algorithm and its implementation using GPU programming.

Table 1 summarizes the runtime achieved to perform the simulations described above using our GPU-OkMC. Results were obtained for $\omega = 1$ (See Eq. 3). For comparison, we also reported the runtimes achieved using the CPU-based OkMC LAKIMOCA code. As we can see, our algorithm shows a significant speedup in the range [30-40]. It is worth noting that these speedups were achieved using a commercial GPU NVIDIA® GeForce® GTX TITAN Black card with 6 GB of global memory and 2880 CUDA cores. It is expected that even larger speedups could be achieved by simply using a more performant

Simulation temp.	CPU time	GTX TITAN Black time
130 K	64 min	100 s (38.3×)
135 K	98 min	183 s (32.2×)
140 K	132 min	274 s (28.9×)

Table 1: Simulation times achieved by our GPU-OkMC using a NVIDIA® GeForce® GTX TITAN Black card, compared to the runtimes needed by the sequential OkMC code LAKIMOCA using a CPU AMD Opteron 6174@2.2Ghz. Numbers in brackets indicate the corresponding speedup.

ω	0.1	0.5	1.0	2.0	5.0
Speedup	4.5×	17.8×	32.2×	51.1×	115.6×

Table 2: Speedup achieved with our GPU-OkMC algorithm for different values of ω in comparison to LAKIMOCA runtimes for the case $T = 135K$.

GPU, i.e. with more memory and more CUDA cores.

In order to examine the influence of the choice of time step width on accuracy and speedup, as discussed in subsection 2.1, the case $T = 135\ K$ was repeated with different values of ω ranging from 0.1 to 5. As previously, results were compared to the result obtained with LAKIMOCA. The speedup achieved for the different values of ω is reported in Table 2. As we can see, speedup can be significantly improved by reasonably increasing the ω value, i.e. the time step, from 1 to 5. Indeed, larger time step values imply that less computational steps are necessary to reach a specified physical time. It is important to note that simulation results (not shown here) evidenced only a slight deviation of the results for the highest value of ω tested here, i.e. for the largest time step. As mentioned in subsection 2.1, in general we only observed a slight influence of ω on the accuracy, at least in the conditions tested here. Thus, in the tests studied here, it was easy to find a good compromise between performance and accuracy for values of $\omega > 1$.

3.4. Application: Simulation of a resistivity recovery experiment

In order to demonstrate the efficiency of our GPU-OkMC to simulate the evolution of a large amount of interacting particles in realistic conditions, we simulated a typical resistivity recovery (RR) experiment in a Fe sample with realistic dimentions. This type of experiment is of importance as it allows to investigate the kinetics of defects in metals [63, 64, 65]. In a typical RR experiment, the sample is first cooled down to a very low temperature $(4 - 77K)$ and is then irradiated with electrons, such that only Frenkel pairs $(I - V)$ are produced. At these temperatures, self-interstitials and vacancies are immobile and thus their recombination is inhibited. Temperature is then increased by δT and kept constant for a fixed amount of time, in general in the order of a few minutes. Resistivity ρ is measured at the end of the isothermal annealing and the process is repeated until a preset temperature is reached. Since

resistivity reflects the total number of defects that affect electron diffusion in the metal, RR experiments are a valuable tool to study the evolution of defects and the thermally-activated mechanisms they undergo. In practice, a typical RR curve exhibits several drops, reflecting the activation of recombination processes. Indeed, as temperature increases, the migration of the different defects gets thermally activated, allowing them to diffuse and recombine with defects of the opposite type. As a result, if the derivative of the total number of defects is plotted with respect to temperature, a typical RR spectrum exhibits several peaks, also called recovery stages, corresponding to the different thermally-activated mechanisms [15, 38, 57] that take place in the metal.

To simulate a typical RR experiment in Fe, we considered the evolution of SIAs and Vs in pure Fe, assuming that they both migrate and can recombine, as described in previous subsection. The formation of SIA or V clusters or other mechanisms were neglected here. We emphasize that our goal is not to propose a physically-based model to explain the different features of the kinetics of defects in Fe but to show that, taking into account basic mechanisms and Fe parameters, our GPU-OkMC can be used to reproduce typical experiments using realistic simulation boxes representative of real samples with a large amount of particles and in short runtimes.

Here we consider a simulation box similar to that of a typical sample thickness in a RR experiment, with a thickness of about 20 μm ($70000a_0$). For the sake of simplicity, the effect of electron irradiation, i.e. the formation of Frenkel pairs during irradiation, was emulated by distributing randomly an equal number of interstitials and vacancies in the simulation box. In the present case we used 10 million SIAs and 10 million Vs. The evolution of the system was then simulated for temperatures starting from 77 K up to 140 K with increase steps of $\frac{\delta T}{T} = 0.008$, and an annealing time $t = 300$ s at each temperature. Each RR curve simulated here consists thus of 77 simulations at different temperatures. This was done for different values of x_{max} and y_{max}, in order to vary the volume of the simulation box and thus the initial concentration of particles. Like in previous cases, $\omega = 1$ was used to compute time step values.

In Fig. 7, we show the derivative of the total number of defects as a function of temperature for different initial concentrations (different x_{max} and y_{max}). As the figure evidences, two different peaks (or stages) can be observed, depending on the initial concentration. When the initial concentration is sufficiently high, our GPU-OkMC predicts a first peak at about $107K$, which corresponds to the so-called I_D stage reported in literature [57, 32] for Fe. This stage corresponds to the recombination of correlated interstitials and vacancies, i.e. that are spatially close. When the migration of SIAs is thermally activated, the probability that they recombine with their vacancy after the first jump is relatively high, giving rise to a recombination at relatively low temperature. The temperature at which our GPU-OkMC predicts this stage to appear is in perfect agreement with what is observed experimentally [57] and predicted theoretically [32]. Our GPU-OkMC also predicts a second peak at a temperature of about $120-130K$, in very good agreement to what is reported in the literature [57, 32]. In contrast to previous stage (I_D), this stage, commonly denoted stage I_E, corresponds to

the recombination of uncorrelated $I-V$ pairs. It is related to the recombination of interstitials that must perform several jumps before they can find a vacancy and recombine. As one can see in Fig. 7, this peak shifts towards higher temperatures as initial concentration decreases. This is expected and experimentally observed [58] since for lower particle densities, the mean distance between particles increases and thus, interstitials need to perform more jumps to find a vacancy to recombine with. As a result, it becomes more difficult for interstitials to find a vacancy in a limited amount of time as the initial concentration decreases. Hence, higher temperatures are necessary for them to perform the required number of jumps before they can recombine with a vacancy, leading to the shift in temperature of stage I_E.

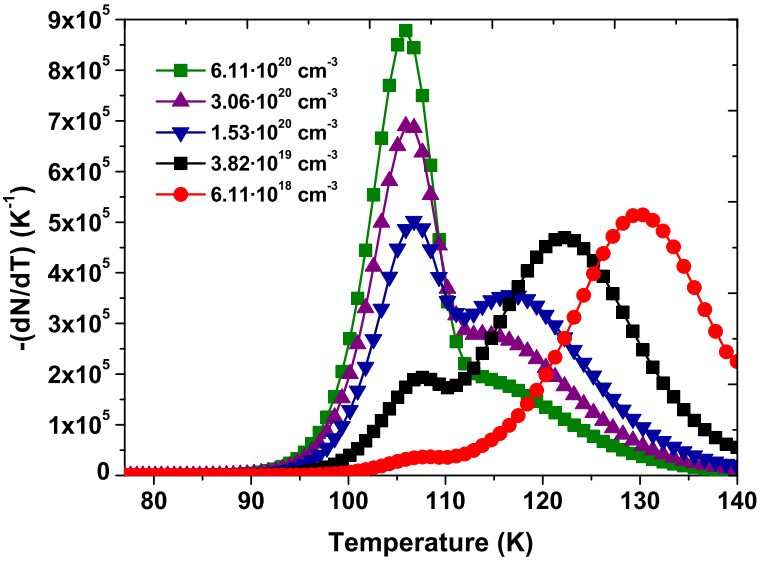

Figure 7: Resistivity recovery spectra corresponding to different initial SIA and V densities.

In Table 3 we reported the runtimes that were necessary to achieve the simulations shown in Fig. 7 for the different initial concentrations, the initial number of particles being 20 million in all cases. As one can see, our GPU-OkMC allows to simulate the evolution of a large number of particles and reproduce a realistic experiment in very reasonable runtimes. Where an OkMC based on the standard BKL algorithm would likely require days of calculations, our parallel OkMC algorithm implemented using GPU programming only requires computational times between 6 min and slightly less than 1 h in the worst case (lowest concentration). Longer runtimes were indeed obtained in the cases where the system is diluted due to the fact that the probability of encounter/recombination

Simulation box	Initial density of defects (cm^{-3})	Runtime (s)
$100a_0 \times 100a_0 \times 70000a_0$	1.22×10^{21}	400.7
$100a_0 \times 200a_0 \times 70000a_0$	6.12×10^{20}	476.6
$200a_0 \times 200a_0 \times 70000a_0$	3.06×10^{20}	631.4
$400a_0 \times 400a_0 \times 70000a_0$	7.64×10^{19}	1270
$1000a_0 \times 1000a_0 \times 70000a_0$	1.22×10^{19}	3481

Table 3: Size of simulation box, initial concentration of defects and respective runtimes corresponding to Fig. 7.

between SIAs and Vs is lower and thus, a larger amount of particles is present in the system during the simulations.

4. Conclusions

In this work we have proposed a parallel Object kinetic Monte Carlo algorithm that was implemented using a GPU programming approach to simulate the evolution of large amounts of interacting particles in materials. In our algorithm, the time step value is first fixed and then the Poisson probability that an event occurs is computed independently and in parallel for each particle. This allows to increase the time step values by orders of magnitude in contrast to the standard BKL algorithm. At the same time, this allows a large fraction of particles to undergo events in parallel during the same time step, in contrast to the standard BKL algorithm that allows only one event to occur per time step. As a result, the number of computational steps to be performed to reach a specified physical time is significantly reduced.

Accuracy and performances of our GPU-OkMC code have been tested under different conditions. In the case of random walks under reflective or absorbing surfaces, the results obtained with our GPU-OkMC are in excellent agreement with those obtained with classical Fick's laws of diffusion. In the case of diffusion of interacting particles, the results obtained with our GPU-OkMC are in excellent agreement with those obtained with a OkMC code based on the standard BKL algorithm. Performances of our GPU-OkMC have been compared to those of a CPU-based OkMC, evidencing speedups in the range [30-40] with constant time step $\delta t = 1/R_{max}$, i.e. for $\omega = 1$. Larger speedups were obtained by using larger values for ω at the expense of a slight loss of accuracy. It must be noted that even higher speedups could be obtained by using a more performant graphics card than the one that was used in the present study.

In order to evidence the usefulness of our GPU-OkMC to simulate realistic experiments, we have reproduced a typical resistivity recovery (RR) experiment assuming an irradiated Fe sample of realistic sizes containing 20 million $I - V$ pairs. By only taking into account the migration and recombination of interstitials and vacancies in Fe, our GPU-OkMC was able to accurately predict the main features of RR spectra in Fe that are observed experimentally and reported in the literature. On average, our GPU-OkMC was able to reproduce a complete

RR experiment with runtimes between 6 min and less than 1 h, when several days of computation would have been necessary with a OkMC code based on the standard BKL algorithm.

We believe this parallel OkMC algorithm implemented using a GPU programming approach will open new possibilities in the investigation of defects in irradiated materials or in other fields of research as it allows now to study the evolution of a large amount of interacting species in samples of realistic dimensions.

5. Acknowledgements

This work has been carried out within the framework of the EUROfusion Consortium and has received funding from the Euratom research and training programme 2014-2018 under grant agreement No 633053. The views and opinions expressed herein do not necessarily reflect those of the European Commission. The authors acknowledge M. Cárdenas from CIEMAT for helpful discussions related to GPU programming and N. Castin from SCK-CEN for valuable discussions on OkMC. The authors also aknowledge C. Domain from EDF for complementary simulations with LAKIMOCA code.

[1] A. S. H. Hameed, S. Rohani, W. C. Yu, C. Y. Tai, C. W. Lan, Surface defects and mechanical hardness of rapidly grown DAST crystals, J. Cryst. Growth 297 (2006) 146–151.

[2] R. Schaeublin, J. Henry, Y. Dai, Materials subjected to fast neutron irradiation, C. R. Physique 9 (2008) 389–400.

[3] F. J. Morin, J. P. Maita, Electrical properties of silicon containing arsenic and boron, Phys. Rev. 96 (1954) 28.

[4] G. L. Pearson, J. Bardeen, Electrical properties of pure silicon and silicon alloys containing boron and phosphorus, Phys. Rev. Lett. 85 (1949) 865.

[5] X. Wu, X. Pan, M. Li, J. F. Stubbins, Modeling tensile response and flow localization effects in 316ss after exposure to spallation and fission irradiation environments, J. Nucl. Mater. 343 (2005) 302–307.

[6] R. Car, M. Parrinello, Unified approach for molecular dynamics and density-functional theory, Phys. Rev. Lett. 55 (1985) 2471.

[7] W. J. Phythian, R. E. Stoller, A. J. E. Foreman, A. F. Calder, D. J. Bacon, A comparison of displacement cascades in copper and iron by molecular dynamics and its application to microstructural evolution, J. Nucl. Mater. 223 (1995) 245–261.

[8] K. Nordlund, M. Ghaly, R. S. Averback, M. J. Caturla, T. D. de la Rubia, J. Tarus, Defect production in collision cascades in elemental semiconductors and fcc metals, Phys. Rev. B 57 (1998) 7556–7570.

[9] A. F. Calder, D. J. Bacon, A molecular dynamics study of displacement cascades in α-iron, J. Nucl. Mater. 207 (1993) 25–45.

[10] J. D. Bacon, T. D. de la Rubia, Molecular dynamics computer simulations of displacement cascades in metals, J. Nucl. Mater. 216 (1994) 275–290.

[11] B. Sadigh, T. J. Lenosky, S. K. Theiss, M. J. Caturla, T. D. de la Rubia, M. A. Foad, Mechanism of boron diffusion in silicon: An ab initio and kinetic Monte Carlo study, Phys. Rev. Lett. 83 (1999) 4341–4344.

[12] C. Becquart, C. Domain, U. Sarkar, A. DeBacker, M. Hou, Microstructural evolution of irradiated tungsten: Ab initio parameterisation of an OKMC model, J. Nucl. Mater. 403 (2010) 75–88.

[13] C. Becquart, A. Barbu, J. L. Bocquet, M. J. Caturla, C. Domain, C.-C. Fu, S. I. Golubov, M. Hou, L. Malerba, C. J. Ortiz, A. Souidi, R. E. Stoller, Modeling the long-term evolution of the primary damage in ferritic alloys using coarse-grained methods, J. Nucl. Mater. 406 (2010) 39–54.

[14] F. Soisson, C. Becquart, N. Castin, C. Domain, L. Malerba, E. Vincent, Atomistic kinetic Monte Carlo studies of microchemical evolutions driven by diffusion processes under irradiation, J. Nucl. Mater. 406 (2010) 55–67.

[15] C. J. Ortiz, M. J. Caturla, Simulation of defect evolution in irradiated materials: Role of intracascade clustering and correlated recombination, Phys. Rev. B 75 (2007) 184101.

[16] E. Vincent, C. S. Becquart, C. Domain, Solute interaction with point defects in α-fe during thermal ageing: A combined ab initio and atomic kinetic Monte Carlo approach, J. Nucl. Mater. 351 (2006) 88–99.

[17] E. Vincent, C. S. Becquart, C. Domain, Atomic kinetic Monte Carlo model based on ab initio data: Simulation of microstructural evolution under irradiation of dilute Fe-CuNiMnSi alloys, Nucl. Instrum. Meth. B 255 (2007) 78–84.

[18] D. Terentyev, G. Bonny, N. Castin, C. Domain, L. Malerba, P. Olsson, V. Moloddtsov, R. C. Pasianot, Further development of large-scale atomistic modelling techniques for Fe–Cr alloys, J. Nucl. Mater. 409 (2011) 167–175.

[19] I. Martín-Bragado, Comprehensive modeling of solid phase epitaxial growth using Lattice Kinetic Monte Carlo, Nucl. Instr. Meth. Phys. Res. B 303 (2013) 184–187.

[20] C. J. Ortiz, P. Pichler, T. Fühner, F. Cristiano, B. Colombeau, N. E. B. Cowern, A. Claverie, A physically based model for the spatial and temporal evolution of self-interstitial agglomerates in ion-implanted silicon, J. Appl. Phys. 96 (2004) 4866–4877.

[21] Y. G. Li, W. H. Zhou, R. H. Ning, L. F. Huang, Z. Zeng, X. Ju, A cluster dynamics model for accumulation of helium in tungsten under helium ions and neutron irradiation, Commun. Comput. Phys. 11 (2012) 1547–1568.

[22] E. Meslin, A. Barbu, L. Boulanger, B. Radiguet, P. Pareige, K. Arakawa, Cluster-dynamics modelling of defects in α-iron under cascade damage conditions, J. Nucl. Mater. 382 (2008) 190–196.

[23] A. Barbu, E. Clouet, Cluster dynamics modeling of materials: advantages and limitations, Solid State Phenom. 129 (2007) 51–58.

[24] T. Jourdan, G. Bencteux, G. Adjanor, Efficient simulation of kinetics of radiation induced defects: A cluster dynamics approach, J. Nucl. Mater. 444 (2014) 298–313.

[25] M. J. Caturla, N. Soneda, E. Alonso, B. D. Wirth, T. D. de la Rubia, J. M. Perlado, Comparative study of radiation damage accumulation in Cu and Fe, J. Nucl. Mater. 276 (2000) 13–21.

[26] H. Xu, Y. N. Osetsky, R. E. Stoller, Cascade annealing simulations of bcc iron using object kinetic Monte Carlo, J. Nucl. Mater. 423 (2012) 102–109.

[27] L. Malerba, C. Becquart, C. Domain, Object kinetic Monte Carlo study of sink strengths, J. Nucl. Mater. 360 (2007) 159–169.

[28] G. J. Galloway, G. J. Ackland, Molecular dynamics and object kinetic monte carlo study of radiation-induced motion of voids and he bubbles in bcc iron, Phys. Rev. B 87 (2013) 104106.

[29] M. Aboy, L. Pelaz, L. A. Marqués, P. López, J. Barbolla, R. Duffy, V. C. Venezia, P. B. Griffin, Role of silicon interstitials in boron cluster dissolution, Appl. Phys. Lett. 86 (2005) 031908.

[30] L. Pelaz, L. A. Marqués, M. Aboy, J. Barbolla, G. H. Gilmer, Atomistic modeling of amorphization and recrystallization in silicon, Appl. Phys. Lett. 82 (2003) 2038.

[31] C. Domain, C. S. Becquart, L. Malerba, Simulation of radiation damage in Fe alloys: an object kinetic Monte Carlo approach, J. Nucl. Mater. 335 (2004) 121–145.

[32] C.-C. Fu, J. D. Torre, F. Willaime, J.-L. Bocquet, A. Barbu, Multiscale modelling of defect kinetics in irradiated iron, Nature Materials 4 (2005) 68–74.

[33] C.-C. Fu, F. Willaime, P. Ordejón, Stability and mobility of mono- and di-interstitials in α-fe, Phys. Rev. Lett. 92 (2004) 175503.

[34] C.-C. Fu, F. Willaime, Interaction between helium and self-defects in α-iron from first principles, J. Nucl. Mater. 367–370 (2007) 244–250.

[35] L. Ventelon, F. Willaime, C.-C. Fu, M. Heran, I. Ginoux, Ab initio investigation of radiation defects in tungsten: Structure of self-interstitials and specificity of di-vacancies compared to other bcc transition metals, J. Nucl. Mater. 425 (2012) 16–21.

[36] E. Zarkadoula, S. L. Daraszewicz, D. M. Duffy, M. A. Seaton, I. T. Todorov, K. Nordlund, M. T. Dove, K. Trachenko, The nature of high-energy radiation damage in iron, J. Phys.: Condens. Matter 25 (2013) 125402.

[37] C. Björkas, K. Nordlund, M. J. Caturla, Influence of the picosecond defect distribution on damage accumulation in irradiated α-fe, Phys. Rev. B 85 (2012) 024105.

[38] D. Terentyev, P. Olsson, T. P. C. Klaver, L. Malerba, On the migration and trapping of single self-interstitial atoms in dilute and concentrated Fe–Cr alloys: Atomistic study and comparison with resistivity recovery experiments, Comp. Mat. Sci. 43 (2008) 1183–1192.

[39] L. Malerba, G. J. Ackland, C. S. Becquart, G. Bonny, C. Domain, S. L. Dudarev, C.-C. Fu, D. Hepburn, M. C. Marinica, P. Olsson, R. C. Pasianot, J. M. Raulot, F. Soisson, D. Terentyev, E. Vincent, F. Willaime, Ab initio calculations and interatomic potentials for iron and iron alloys: Achievements within the Perfect project, J. Nucl. Mater. 406 (2010) 7–18.

[40] R. E. Stoller, S. I. Golubov, C. Domain, C. S. Becquart, Mean field rate theory and object kinetic Monte Carlo: A comparison of kinetic models, J. Nucl. Mater. 382 (2008) 77–90.

[41] W. Cai, V. V. Bulatov, J. ao F. Justo, A. S. Argon, S. Yip, Kinetic Monte Carlo approach to modeling dislocation mobility, Comp. Mat. Sci. 23 (2002) 124–130.

[42] A. B. Bortz, M. H. Kalos, J. L. Leibowitz, A new algorithm for Monte Carlo simulation of Ising spin systems, J. Comp. Phys. 17 (1975) 10–18.

[43] D. T. Gillespie, A general method for numerically simulating the stochastic time evolution of coupled chemical reactions, J. Comput. Phys. 22 (1976) 403.

[44] A. F. Voter, Introduction to the kinetic Monte Carlo method, in: K. E. Sickafus, E. A. Kotomin, B. P. Uberuaga (Eds.), Radiation Effects in Solids, Springer, Dordrecht, Netherlands, 2007.

[45] J. Wei, F. E. Kruis, GPU-accelerated Monte Carlo simulation of particle coagulation based on the inverse method, J. Comp. Phys. 249 (2013) 67–79.

[46] M. A. Tschopp, K. N. Solanki, F. Gao, X. Sun, M. A. Khaleel, M. F. Horstemeyer, Probing grain boundary sink strength at the nanoscale: Energetics and length scales of vacancy and interstitial absorption by grain boundaries in α-fe, Phys. Rev. B 85 (2012) 064108.

[47] X.-M. Bai, A. F. Voter, R. G. Hoagland, M. Nastasi, B. P. Uberuaga, Efficient annealing of radiation damage near grain boundaries via interstitial emission, Science 327 (2010) 1631–1634.

[48] G. S. Was, J. P. Wharry, B. Frisbie, B. D. Wirth, D. Morgan, J. D. Tucker, T. R. Allen, Assessment of radiation-induced segregation mechanisms in austenitic and ferritic–martensitic alloys, J. Nucl. Mater. 411 (2011) 41–50.

[49] T. Allen, J. Cole, J. Gan, G. Was, R. Dropek, E. Kenik, Swelling and radiation-induced segregation in austenitic alloys, J. Nucl. Mater. 342 (2005) 90–100.

[50] J. Busby, G. Was, E. Kenik, Isolating the effect of radiation-induced segregation in irradiation-assisted stress corrosion cracking of austenitic stainless steels, J. Nucl. Mater. 302 (2002) 20–40.

[51] D. Terentyev, X. He, E. Zhurkin, A. Bakaev, Segregation of Cr at tilt grain boundaries in Fe–Cr alloys: A Metropolis Monte Carlo study, J. Nucl. Mater. 408 (2011) 161–170.

[52] K. Arakawa, H. Mori, K. Ono, Formation process of dislocation loops in iron under irradiations with low-energy helium, hydrogen ions or high-energy electrons, J. Nucl. Mater. 307 (2002) 272–277.

[53] E. Martínez, J. Marian, M. H. Kalos, M. Preciado, Synchronous parallel kinetic Monte Carlo for continuum diffusion-reaction systems, J. Comp. Phys. 227 (2008) 3804–3823.

[54] C. Navarro, N. Hitschfeld-Kahler, L. Mateu, A survey on parallel computing and its applications in data-parallel problems using GPU architectures, Commun. Comput. Phys. 15 (2014) 285–329.

[55] R. Farber, CUDA Application Design and Development, Morgan Kaufmann, Waltham, USA, 2011.

[56] B. Gómez-Ferrer, R. Vila, D. Jiménez-Rey, C. J. Ortiz, F. Mota, J. M. García, A. Rodríguez, In situ resistivity measurements of RAFM base alloys at cryogenic temperatures: The effect of proton irradiation, J. Nucl. Mater. 447 (2014) 225–232.

[57] S. Takaki, J. Fuss, H. Kugler, U. Dedek, H. Schultz, The resistivity recovery of high purity and carbon doped iron following low temperature electron irradiation, Radiation Effects 79 (1983) 87–122.

[58] H. Matsui, S. Takehana, M. W. Guinan, Resistivity recovery in high purity iron after fission- and fusion- neutron irradiation, J. Nucl. Mater. 155-157 (1988) 1284–1289.

[59] J. D. Torre, C.-C. Fu, F. Willaime, A. Barbu, J.-L. Bocquet, Resistivity recovery simulations of electron-irradiated iron: Kinetic Monte Carlo versus cluster dynamics, J. Nucl. Mater. 352 (2006) 42–49.

[60] D. T. Gillespie, Approximate accelerated stochastic simulation of chemically reacting systems, J. Chem. Phys. 115 (2001) 1716.

[61] S. L. Grand, Broad-phase collision detection with CUDA, in: N. Corporation (Ed.), GPU Gems 3, 2008.

[62] S. Chandrasekhar, Stochastic problems in physics and astronomy, Rev. Mod. Phys 15 (1943) 1–89.

[63] A. L. Nikolaev, T. E. Kurennykh, On the interaction between radiation-induced defects and foreign interstitial atoms in α-iron, J. Nucl. Mater. 414 (2011) 374–381.

[64] H. Abe, E. Kuramoto, Recovery of electrical resistivity of high-purity iron irradiated with 30 MeV electrons at 77 K, J. Nucl. Mater. 283-287 (2000) 174–178.

[65] A. L. Nikolaev, Stage I of recovery in 5 MeV electron-irradiated iron and iron–chromium alloys: the effect of small cascades, migration of di-interstitials and mixed dumbbells, J. Phys.: Condens. Matter 11 (1999) 8633–8644.